Mechanism of substrate inhibition in cytochrome-c dependent NO reductases from denitrifying bacteria (cNORs)

Matsumura, Hirotoshi; Faponle, Abayomi S.; Hagedoorn, Peter Leon; Tosha, Takehiko; de Visser, Sam P.; Moënne-Loccoz, Pierre

DOI
10.1016/j.jinorgbio.2022.111781

Publication date
2022

Document Version
Final published version

Published in
Journal of Inorganic Biochemistry

Journal of Inorganic Biochemistry 231 (2022) 111781

Contents lists available at ScienceDirect

Journal of Inorganic Biochemistry

journal homepage: www.elsevier.com/locate/jinorgbio

Mechanism of substrate inhibition in cytochrome-c dependent NO reductases from denitrifying bacteria (cNORs)

Hirotoshi Matsumura [a,1], Abayomi S. Faponle [b,2], Peter-Leon Hagedoorn [c], Takehiko Tosha [d], Sam P. de Visser [b], Pierre Moënne-Loccoz [a,*]

[a] Department of Chemical Physiology and Biochemistry, School of Medicine, Oregon Health & Science University, 3181 SW Sam Jackson Park Road, Portland, OR 97239, USA
[b] Manchester Institute of Biotechnology, Department of Chemical Engineering and Analytical Science, The University of Manchester, 131 Princess Street, Manchester M1 7DN, United Kingdom
[c] Department of Biotechnology, Delft University of Technology, Van der Maasweg 9, 2629 HZ Delft, the Netherlands
[d] RIKEN SPring-8 Center, 1-1-1, Kouto, Sayo, Hyogo 679-5148, Japan

ARTICLE INFO

Keywords:
Nitric oxide reductases
Iron proteins
Spectroscopy
Reaction mechanisms

ABSTRACT

Steady-state kinetics of cytochrome-c dependent denitrifying NO reductases (cNORs) show evidence of substrate inhibition at NO concentrations higher than 10 μM, but the mechanism of inhibition remains unclear. Here, we present low-temperature FTIR photolysis experiments carried out on the NO complex formed by addition of NO to the oxidized cNORs. A differential signal at 1261 cm^{-1} that downshifts with ^{15}NO and $^{15}N^{18}O$ is assigned to a $\nu(NO_2)$ from a bridging diiron-nitrito complex at the heme-nonheme diron site. Theoretical calculations reproduces observed frequencies and isotope shifts. Our experimental results confirm a prior theoretical study by Blomberg and Siegbahn [Blomberg, M. R., and Siegbahn, P. E. M. *Biochemistry* 2012, *51*, 5173–5186] that proposed substrate inhibition through a radical combination reaction between the diferric μ-oxo group and an NO molecule to form a heme Fe(III)-nitrito-Fe_B(II) inhibitory complex. Stopped-flow experiments suggest that substrate inhibition also occurs after a half-reduction cycle, i.e. when fully-reduced cNOR reduces two NO molecules at the heme-nonheme diferrous active site cluster to produce one N_2O molecule and the diferric cluster. These results support catalytic mechanisms that proceed through isomerization of a diferric-hyponitrite transient complex to produce a bridging diferric μ-oxo group and N_2O without protonation of the putative hyponitrite intermediate.

1. Introduction

Denitrifying NO reductases are integral membrane proteins structurally and functionally related to the respiratory terminal oxidases. In contrast with terminal oxidases that utilize a heme/copper binuclear active site to reduce O_2 to H_2O, denitrifying NO reductases depend on a heme/nonheme diiron cluster to reduce two NO molecules to N_2O. This reaction is an essential step of the anaerobic respiration of denitrifying bacteria and it also contributes to the scavenging of NO, which leads to virulence in many bacterial pathogens, including *Pseudomonas aeruginosa (P.a.), Neisseria meningitis* and *N. Gonorrhoeae*, and *Brucella melitensis* [1–4].

Prior to the 2010 publication of the crystal structure of *P.a.* cytochrome-c dependent nitric oxide reductase (cNOR) [5], resonance Raman (RR) spectroscopy provided the first direct evidence for the presence of a heme-nonheme diferric cluster, known as the heme b_3-nonheme Fe_B cluster. Specifically, RR spectra of air-oxidized *Paracoccus denitrificans (P.d.)* cNOR obtained with a 442-nm excitation exhibit an intense vibration at 810 cm^{-1} that downshifts 40 cm^{-1} after exposure to $^{18}OH_2$, supporting its assignment to the asymmetric stretching vibration

Abbreviations: cNOR, cytochrome-c dependent NO reductase; 5cHS, pentacoordinnate high-spin; RFQ, rapid-freeze-quench; EPR, electron paramagnetic resonance; RR, resonance Raman; FTIR, Fourier transform infrared; DFT, density functional theory.

* Corresponding author.
E-mail address: moennelo@ohsu.edu (P. Moënne-Loccoz).
[1] Current address: Department of Life Science, Graduate School of Engineering Science, Akita University, 1-1 Tegata Gakuen-machi, Akita City, Akita, 010-8502 Japan.
[2] Current address: Department of Biochemistry, Faculty of Basic Medical Sciences, Olabisi Onabanjo University, Sagamu Campus, Ogun State, Nigeria.

https://doi.org/10.1016/j.jinorgbio.2022.111781
Received 28 November 2021; Received in revised form 21 February 2022; Accepted 24 February 2022
Available online 1 March 2022

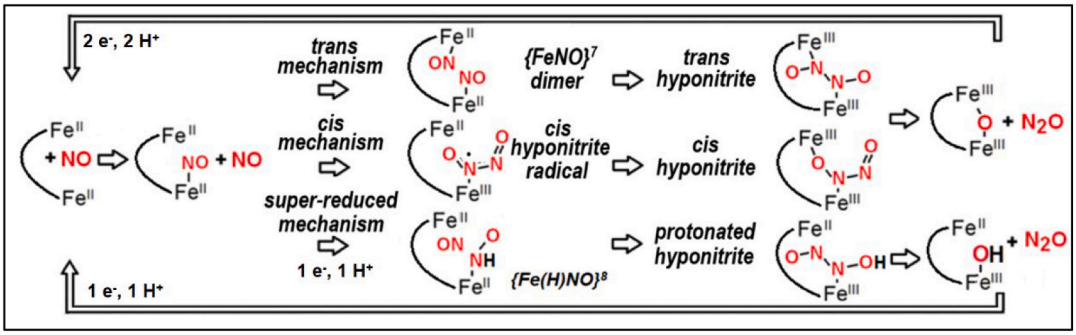

Scheme 1. Possible mechanisms of NO reduction at diferrous metal clusters.

of a solvent exchangeable bridging μ-oxo group, ν_{as}(Fe-O-Fe) [6]. A diferric heme-nonheme diiron synthetic model composed of a tris(2-pyridylmethyl)amine moiety tethered to a synthetic porphyrin [7] provided an ideal mimic, exhibiting an equivalent ν_{as}(Fe-O-Fe) at 841 cm^{-1}, and confirming that these RR frequencies could be used to conclude that the active site of cNORs anchored a diferric cluster with an Fe-O-Fe angle of ~145° and Fe – Fe distance ≤3.5 Å [6]. A prior RR characterization further defined the active site heme b_3 as a penta-coordinate high-spin (5cHS) species in both oxidized and reduced states of the enzyme [8].

The crystal structure of *P.a.* cNOR, refined at 2.7-Å resolution, revealed an oxo-bridged diiron cluster with a 3.8 Å Fe—Fe distance, and a hexacoordinate heme iron with a proximal histidine at 2.3 Å. The optical absorption spectra obtained on the crystal after 30 s of X-ray irradiation suggested partial photoreduction [5], which may explain the apparent discrepancy between the RR and X-ray data. However, it is worth noting that air-oxidized *P.d.* cNOR can be purified in its canonical form characterized by a high-spin charge transfer absorption feature at 596 nm assigned to the 5cHS heme b_3 [8,9], as well as in an alternative conformer that almost entirely lacks the 596-nm absorption feature, reproducing more closely the UV–vis spectra of oxidized *P.a.* cNOR [5,10], and suggesting a hexacoordinate configuration of the ferric heme b_3 in *P.a.* cNOR. Because synthetic porphyrin diferric μ-oxo complexes seem to enforce 5cHS configurations and to preclude coordination trans to the oxo group, a His-(porphyrin)Fe(III)-O-Fe_B(III) cluster may be another example of an entatic state (for a recent discussion of entatic states see [11]).

Our characterization of the heme/nonheme diferric μ-oxo bridge in *P.d.* cNOR and in synthetic model compounds led us to propose a minimalistic reaction mechanism with binding of one NO molecule to each iron(II) center and formation of an N—N bond between the resulting iron(III)-nitroxyl complexes, before rearrangement of the resulting hyponitrite dianion complex to lead to N—O bond cleavage with production of N_2O and the μ-oxo bridging ligand; in this mechanistic model called *trans* mechanism, proton events are limited to the re-reduction step of the diferric site and release of the μ-oxo bridge as a water molecule (Scheme 1) [8,12]. Theoretical models of this reaction by Blomberg and Siegbahn favor a *cis* mechanism involving the reaction of a heme-nitrosyl complex with a second NO to produce a bridging cis-hyponitrite intermediate before rearrangement of the hyponitrite with a bridging oxo-group leading to N—O bond cleavage [13–15]. While these two mechanisms differ in terms of the binding steps for the two NO molecules, they both implicate the diferric μ-oxo cluster as the product of a single turnover and restrict the requirement of proton to the re-reduction of the diferric cluster. However, mechanisms involving reduction of nitrosyl to nitroxyl species, and protonation of nitroxyl or hyponitrite intermediates remain attractive alternatives [16,17].

Demonstrating that the 5-coordinate μ-oxo bridged ferric heme structure corresponds to the product of the catalytic turnover could be experimentally confirmed by the retention of an O-atom from NO at the μ-oxo group and would be a strong vindication for the *trans* or *cis* mechanism (Scheme 1). Previous stopped-flow and rapid-freeze-quench EPR (RFQ-EPR) with *P.a.* cNOR have revealed submillisecond single turnover kinetics [18], while RR experiments have shown that the diferric μ-oxo bridge of *P.d.* cNOR exchange with $^{18}OH_2$ occurs with a $t_{1/2}$ of 5 min at room temperature [6]. Thus, it is reasonable to assume that RFQ-RR experiments could be used to probe the formation of the diferric μ-oxo bridge, monitoring the appearance of a ν_{as}(Fe-^{18}O-Fe) upon exposure of fully reduced cNOR to excess $^{15}N^{18}O$ substrate. Here, we show that the high reactivity of the oxidized active site toward NO complicates stopped-flow and RFQ-RR experiments, but low-temperature FTIR experiments identify the mechanism of substrate inhibition in cNOR and provide indirect evidence in support of the diferric μ-oxo bridge as the product of a single turnover.

Substrate inhibition in cNORs is readily apparent from decreasing turnover numbers at NO concentrations beyond ~10 μM in steady-state measurements [9,19]. Early proposals suggested that inhibition occurs through reaction of the oxidized enzyme with NO [9,19], but the molecular details of this reaction were not defined. On the basis of RR and FTIR data, Varotsis and coworkers assigned *P.d.* cNOR's substrate inhibition to the formation of a heme b_3 ferric-nitrosyl complex [20], but multiple attempts in our hands failed to reproduce these spectroscopic data. Here, we describe experimental evidence supporting inhibition through the reaction of NO with the diferric μ-oxo bridge to form a bridging nitrite complex, an inhibition mechanism previously proposed by Blomberg and Siegbahn on the basis of theoretical calculations [14].

2. Material and methods

P.d. cNOR was purified as previously reported and stored at pH 7.0 in 20 mM potassium phosphate or 4-(2-hydroxyethyl)-1-piperazineethanesulfonic acid (HEPES) buffer with 0.05% lauryl maltoside under liquid nitrogen [9]. *P.a.* cNOR was purified as previously reported and stored at pH 7 in 20 mM HEPES buffer with 150 mM NaCl and 0.02% lauryl maltoside [21]. Reduced cNOR was prepared by addition of microliter aliquots from a ~ 5 mM dithionite solution to reach a ~ 8 fold molar excess of dithionite relative to cNOR.

NO solutions were prepared using NO (99.5%, Airgas) and ^{15}NO gas (>98% ^{15}N, Cambridge Isotope Laboratory), and $^{15}N^{18}O$ gas (>98% ^{15}N, >95% ^{18}O, Aldrich), further purified by bubbling through 1 M NaOH solutions to remove the degradation products N_2O_3 and NO_2. All procedures were performed inside an anaerobic glove box containing less than 1 ppm O_2 (Omnilab System, Vacuum Atmospheres Co.). The purified gases were drawn with gas-tight Hamilton syringes and bubbled through buffer solutions in serum bottles fitted with septa. After 5 min of mixing, the NO concentration in the buffered solutions reached the expected NO saturation concentration of ~2 mM. The exact NO concentration was determined each time by titration against deoxymyoglobin.

Stopped-flow experiments were performed with an SX20 apparatus (Applied Photophysics) with a 1-cm path length cell equilibrated at 4 °C inside an anaerobic glove box containing less than 1 ppm O_2 (Nexus System, Vacuum Atmospheres Co.). *P.d.* cNOR stock solutions were

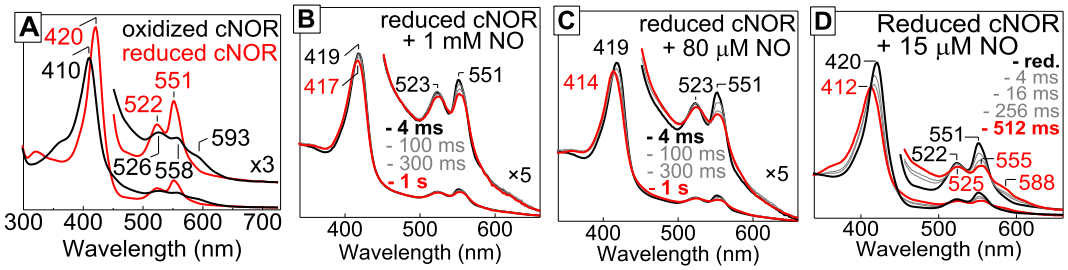

Fig. 1. UV–vis spectra of oxidized and reduced cNOR (*A*) and stopped-flow traces following the exposure of fully reduced cNOR to varying concentrations of NO (*B*, 1 mM NO; *C*, 80 μM NO; D, 15 μM NO). All spectra were obtained at room temperature with 2 μM *P.d.* cNOR in 20 mM potassium phosphate buffer, pH 7.0 with 0.05% lauryl maltoside.

diluted to obtain a final protein concentration of 2 μM in 20 mM potassium phosphate buffer, pH 7.0 with 0.05% lauryl maltoside. NO solutions ranging from ~0.15 to 900 μM in the same buffer were prepared in 1.2 mL glass vials capped with tight septa and were used immediately. Estimates of rate constants were derived from single-exponential fits.

Exposure of oxidized cNOR was performed in Eppendorf tubes prior to transfer in Raman capillaries or FTIR cells. The success of the reaction was confirmed by UV–vis spectra collected directly in Raman capillaries or FTIR cells using a Cary 50 spectrometer.

RR spectra were recorded at either room temperature or 110 K using a custom McPherson 2061/207 spectrograph (set at 0.67-m or 1-m focal length with 2400 grooves per mm holographic gratings) equipped with a liquid-N_2-cooled CCD detector (LN-1100 PB, Princeton Instruments). The 407-nm excitation laser was derived from a Kr laser (Innova 302C, Coherent). A Kaiser Optical supernotch filter or a long-pass filter (RazorEdge, Semrock) was used to attenuate Rayleigh scattering. Room temperature RR spectra were collected in a 90° scattering geometry on samples mounted on a reciprocating translation stage. Frequencies were calibrated relative to indene, which are accurate to ±1 cm^{-1}. Polarization conditions for room temperature RR spectra were optimized using CCl_4 and indene. The integrity of the RR samples was confirmed by direct monitoring of their UV–vis absorption spectra in Raman capillaries or NMR tubes before and after laser exposure. Low-temperature spectra were recorded in a backscattering geometry on samples maintained at 110 K in a liquid nitrogen coldfinger. Frequencies were calibrated relative to aspirin and are accurate to ±1 cm^{-1}. To assess the photosensitivity of the NO adducts, rapid acquisitions within a range of laser powers and continuous sample translation or spinning were compared with longer data acquisitions on static samples. Rather than aiming for maximum signal/noise ratio, RR spectra were obtained with minimal laser power and exposure times to insure the integrity of the samples and prevent ligand photodissociation and laser-induced photoreduction.

2.1. FTIR photolysis experiments

Low-temperature FTIR photolysis was conducted using a previously described method [22–26]. FTIR films were prepared by loading approximately 15 μL of 300 μM protein solution onto an FTIR cell with a 15-μm Teflon spacer. After confirming the formation of the NO adduct by UV − vis absorption spectroscopy, the FTIR cell was mounted to a sample rod which was then flash-frozen in liquid N_2 and inserted into the sample compartment of a pre-cooled closed-cycle cryogenic system (Omniplex, Advanced Research Systems). The cryostat was placed inside the sample compartment of the FTIR and the sample was kept in the dark until the sample well inside the cryostat stabilized to 15 K. The temperature of the sample was monitored and controlled with a Lake Shore Model 331 unit. FTIR spectra were recorded with sets of 1000-scan accumulations at 4-cm^{-1} resolution. Photolysis was performed by continuous illumination of the sample directly in the FTIR sample chamber using the 407-nm laser line a Kr laser (Innova 302C, Coherent). The 200-mW laser beam was defocused to illuminate the entirety of the IR film. The photolysis process was relatively inefficient and more than 10 min of illumination at 15 K was required to maximize the FTIR differential signals. The full reversibility of the photoprocess was confirmed by raising the temperature of the samples to 230 K before lowering the temperature back to 15 K to collect new photoinduced difference spectra that match those observed prior to this annealing process.

2.2. DFT calculations

All density functional theory (DFT) calculations were performed using Gaussian 09 [27]. Following previously benchmarked methods [28,29], the UB3LYP functional was used for geometry optimizations and frequency calculations [30]. These calculations used a double-ζ quality LACVP basis set on iron with electron core potential and 6–31 + G* on all other atoms, basis set B1 [31]. The initial structure used the optimized geometry of Blomberg and Siegbahn [14] reoptimized in Gaussian with the ligands to Fe_B truncated as three methylimidazole and one propionate. No constraints were put on any of the atoms in the models. Three models were investigated: one was a nitrite bridging the two iron ions, one where NO is bound at heme b_3 and water at the Fe_B ion, and a final structure with a μ-oxo bridged diiron complex. After geometry optimization, structures were confirmed as local minima through an analytical frequency calculation that produced only real frequencies; both IR and Raman activities were investigated.

3. Results and discussion

3.1. Stopped-flow UV–vis analysis of the reaction of fully reduced cNOR with NO and evidence for substrate inhibition

Steady-state measurements of NO consumption by cNOR provide evidence for substrate inhibition but the mechanism of this inhibitory effect remains uncertain. Fig. 2 shows stopped-flow UV–vis traces for the reaction of fully-reduced *P.d.* cNOR (2 μM final concentration) with various NO concentrations. Remarkably, at 1 mM or 80 μM NO, the UV–vis absorption changes are minimal, with a small blue shift of the Soret absorption and minimal absorption decreases in the heme α/β absorption region (Fig. 1). These data indicate that, in these conditions of high NO concentrations, the low-spin heme *c* and heme *b* remain in the ferrous states since oxidation of these low-spin hemes is associated with the loss of the distinctive absorption features at 551 and 523 nm [9,18,32,33]. The blue shift of the Soret maximum must relate to NO reactions occurring at the heme b_3 site, but because the 593-nm absorption band characteristic of ferric high-spin b_3 is lacking, the heme b_3 must be in an inhibitory low-spin state that prevent further reaction. Importantly, dropping the NO concentration at or below 15 μM results in clear spectral changes supporting the oxidation of the low-spin hemes with a k_{obs} ~ 13 s^{-1} at 4 °C (Fig. 1). This observed rate would lead to a turnover rate of ~50 NO molecules per second in steady-state conditions

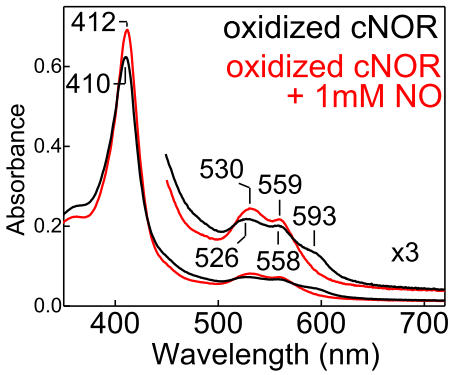

Fig. 2. Room-temperature UV–vis spectra of oxidized *P.d.* cNOR (2 μM) before and after exposure to 1 mM NO.

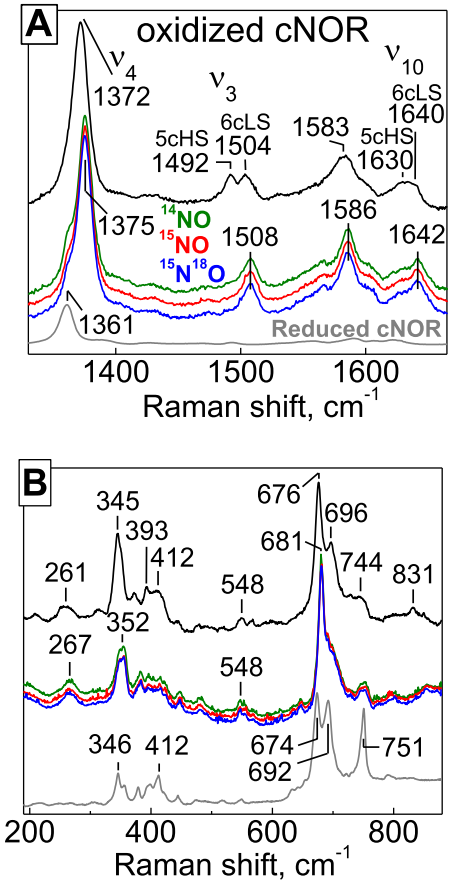

Fig. 3. High- (*A*) and low-frequency (*B*) regions of the RR spectra of oxidized cNOR (top black traces), oxidized cNOR exposed to 1 mM NO (middle traces; unlabeled NO, green traces; ^{15}NO, red traces; $^{15}N^{18}O$, blue traces), and dithionite-reduced cNOR (bottom grey traces). All spectra were collected at room temperature with a 407-nm excitation using 100 μM *P.d.* cNOR solutions in 20 mM potassium phosphate buffer, pH 7.0 with 0.05% lauryl maltoside. (For interpretation of the references to colour in this figure legend, the reader is referred to the web version of this article.)

where the internal electron transfer between ferrous low-spin hemes and the diferric active site is rate limiting, a value that compares well with previous published turnover numbers for various cNORs [5,9,34,35]. The final traces in these stopped-flow experiments at low NO concentrations do not exactly match the spectrum of oxidized cNOR but resemble instead those of oxidized cNOR exposed to NO (Fig. 2),

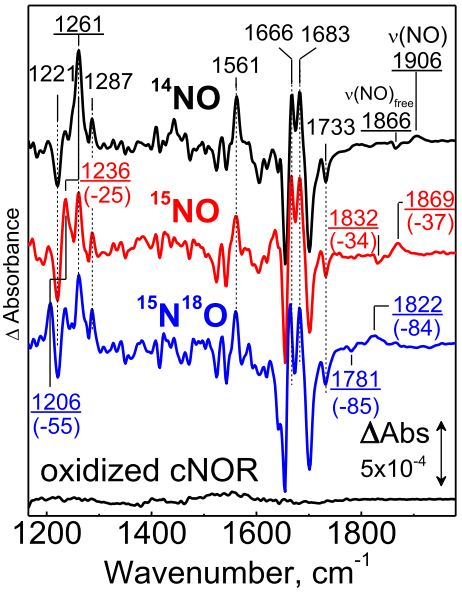

Fig. 4. Low-temperature FTIR photolysis difference spectra of oxidized cNOR exposed to 1 mM NO (top black trace, unlabeled NO; red trace, ^{15}NO; blue trace $^{15}N^{18}O$). A control experiment with oxidized cNOR is also shown (bottom black trace). All samples were prepared inside an anaerobic glovebox, using solutions of 250 μM *P.d.* cNOR exposed for ~2 min to 1 mM NO at room temperature before transfer to sealed IR cell and freezing by immersion in liquid nitrogen (see Material and Method for additional details). (For interpretation of the references to colour in this figure legend, the reader is referred to the web version of this article.)

suggesting that remaining NO reacts further with oxidized cNOR. Thus, our data suggest that at high NO concentration, a first half-reaction produces the diferric [heme b_3:nonheme Fe_B] active site that reacts further with a third NO molecule within the dead-time of the stopped-flow instrument to form a new species where the heme b_3 is a low-spin ferric species, non reduceable by the low-spin ferrous hemes *b* and *c*.

3.2. UV–vis and resonance Raman analysis of the reaction of oxidized cNOR with NO

Anaerobic exposure of oxidized cNOR to excess NO results in modest UV–vis absorption changes. Specifically, the Soret absorption increases marginally with an upshift from 410 to 412 nm with a concomitant gain in absorbance in the Q bands at 559 and 530 nm and loss of the 595-nm shoulder assigned to the ferric high-spin heme b_3 (Fig. 2).

Room-temperature RR spectra of ferric cNOR exposed to excess NO shifts the fully symmetric porphyrin modes ν_4, ν_3 and ν_{10} modes of the 5cHS heme b_3 at 1372, 1492, and 1630 cm^{-1}, respectively to typical frequencies of 6-coordinate low-spin ferric heme species already exhibited by the two low-spin hemes *b* and heme *c* anchored in cNOR, i.e. ν_3 at 1508 and ν_{10} at 1642 cm^{-1} (Fig. 3).

No isotope sensitive mode could be detected with ^{15}NO or $^{15}N^{18}O$ labeled gas (Fig. 3), which contrast with the RR spectra reported by Varotsis and coworkers showing an isotope sensitive band at 594 cm^{-1} which was assigned to a ν(FeNO) from a ferric heme b_3 nitrosyl complex [20].

3.3. Low-temperature FTIR photolysis analysis of the reaction of oxidized cNOR with NO

Seminal experiments with the carbonyl complexes of myoglobins and terminal oxidases have shown how the photolabile character of these adducts could be used to trap dissociated states at cryogenic

temperatures and to extract ν(CO) frequencies of the bound and dissociated states from "dark" minus "illuminated" difference spectra [36–39]. Similar photolysis approaches have been subsequently used to characterize other heme and nonheme labile iron complexes with exogenous ligands, including nitrosyl [26,40–44], azido and nitro complexes [23,45].

As expected, FTIR spectra of oxidized cNOR obtained at 15 K before and after monochromatic illumination of the samples at 407-nm reveal no light-induced differential signal (Fig. 4), confirming that the endogenous ligands to the low-spin hemes and the μ-oxo ligand to the heme b_3 are not photolabile ligands that can be trapped as dissociated species at 15 K. Control experiments with NO saturated buffer solutions also show flat "dark" minus "illuminated" FTIR difference spectra (data not shown). In contrast, the light-induced FTIR difference spectra of oxidized *P.d.* cNOR samples treated with NO are rich in differential signals (Fig. 4). The same 15-K light-induced difference spectra can be obtained again from the same if the sample temperature is raised above 200 K before returning to 15 K. These annealing procedures imply that the photoevents probed by the FTIR difference spectra are fully reversible, but they also indicate that the rebinding process faces a large energy barrier that must include significant reorganization energy of metal endogenous ligands. Accordingly, the vast majority of the differential FTIR signals are unaffected by the isotopic labeling of NO and must therefore reflect conformational changes of the metal endogenous ligands and porphyrin moieties upon exogenous ligand dissociation. Beyond these differential signals, a few FTIR signals exhibit downshifts with heavier NO isotopes.

The most intense positive signal with sensitivity to the labeling of NO is observed at 1261 cm^{-1}. The frequency of this mode and its 25 and 55 cm^{-1} downshifts with ^{15}NO and $^{15}N^{18}O$, respectively, identify this signal as an N—O stretch with partial double bond character as expected for a $\nu(NO_2)$ mode from an Fe(III)-nitrite complex (Fig. 4). Because we use here a monochromatic light source that matches the Soret absorption of the heme cofactors in *P.d.* cNOR, it is reasonable to assume that photolysis is initiated through a porphyrin excited state, leading to reversible dissociation of a nitrite adduct. If illumination of the adduct was to result in an isomerization of the nitrite adduct, we would anticipate observing negative $\nu(NO_2)$ mode corresponding to the new ligand geometry, but we observe no isotope-sensitive negative bands in the expected range for $\nu(NO_2)$ modes. In contrast, a free nitrite anion docked near the diiron site would be expected to present only very weak and broadened vibrations and remain undetectable over the large background differential signals associated with the conformational rearrangement of the endogenous sidechain ligating the diiron cluster upon nitrite dissociation.

Vibrational studies of Fe(III)-porphyrin-nitrite species have shown that 6-coordinate nitro complexes show $\nu_s(NO)$ and $\nu_{as}(NO)$ around 1300 and 1400 cm^{-1}, respectively, while these same modes are observed around 1000 and 1500 cm^{-1} in nitrito complexes [46,47]. Here, only one $\nu(NO_2)$ mode is observed at 1261 cm^{-1}, but a second $\nu(NO_2)$ mode may be too weak to detect or may occur below 1100-cm^{-1}, a spectral region inaccessible in our experiments because of the lack of transmittance from the CaF_2 windows of our cryostat and IR cell.

At the other frequency end for N—O stretch, a positive band at 1906 cm^{-1} that downshifts 37 cm^{-1} with ^{15}NO and 84 cm^{-1} with $^{15}N^{18}O$ is easily observed despite its weak intensity because of the lack of protein moiety vibrations in this spectral range (Fig. 4). This 1906-cm^{-1} frequency is consistent with a N—O stretch from a ferric low-spin heme-nitrosyl, and within 2-cm^{-1} of the ν(NO) reported by Varotsis and coworkers in their earlier work with *P.d.* cNOR [20]. As expected, the positive ν(NO) signals are accompanied by very weak negative bands at 1866, 1832 and 1781 cm^{-1} for NO, ^{15}NO and $^{15}N^{18}O$, respectively, that correspond to the ν(NO) of the dissociated NO ligands docked inside the active site and trapped at cryogenic temperatures. The low absorptivity of ν(NO) modes from NO molecule docked inside the active site versus bound to the heme Fe(III) reflects the low electric dipole of the unligated

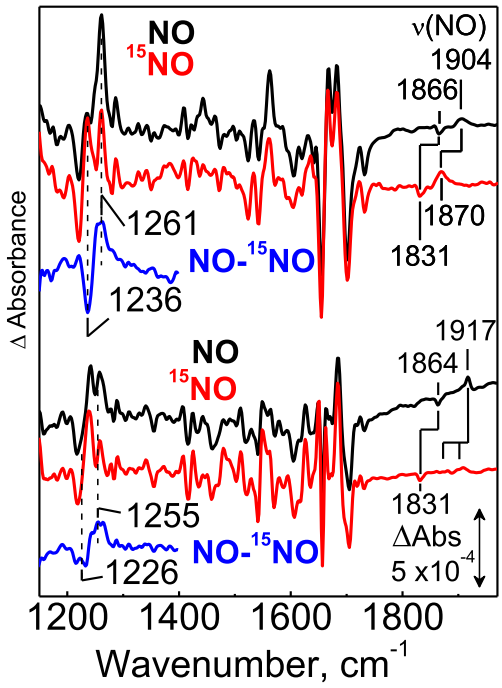

Fig. 5. Comparison of low-temperature FTIR photolysis difference spectra for *P.d.* cNOR (top traces) and *P.a.* cNOR (bottom traces) after exposure to unlabeled NO (black traces) and ^{15}NO (red traces).

NO group, as previously seen in other heme and nonheme iron-nitrosyl cryogenic FTIR photolysis experiments [26,41,43,44,48,49]. For example, in cytochrome bo_3 of *Escherichia coli* photolysis of NO bound at the heme-copper center at cryogenic temperatures lead to the appearance of a ν(NO) at 1863 cm^{-1} that is ~150 weaker than its heme-bound counterpart [25].

Correlating relative intensities between nitrosyl ν(NO) and nitrite $\nu(NO_2)$ modes observed here with relative populations would require to determine, or at least estimate, relative extinction coefficients for these different vibrational modes and relative photolysis efficiencies for these different species. Typically, monitoring the UV–vis absorption spectrum of the IR film before and after photolysis can provide an estimate of the photolysis efficiency, but the differences in UV–vis absorbance of *P.d.* cNOR before and after exposure to NO are too small to contribute to this analysis. Because we use continuous and prolonged illumination, the extent of photodissociation will depend on the efficiency of the cryotrapping of the photodissociated states rather than the quantum yield of photolysis for the nitrite and nitrosyl ligands.

Despite these limitations in interpreting intensities in these FTIR photolysis experiments, comparing the intensities of the ν(NO) of the iron-nitrosyl species and the $\nu(NO_2)$ of the iron-nitrite complex with prior studies clearly supports assigning the nitrite adduct as the major contributor to photolysis. Indeed, after correction for protein concentration and pathlength, the intensity of the positive $\nu(NO_2)$ band seen here is twice as intense as the $\nu(NO_2)$ we recently detected in photolysis experiments with a homogenous heme-nitro complex of cytochrome c' protein [45]. In contrast, the ν(NO) band we observe here at 1906 cm^{-1} is ~4 times weaker than the ν(NO) at 1904-cm^{-1} reported by Varotsis and coworkers for their cNOR heme b_3-nitrosyl [20].

Positive bands at 1561, 1666 and 1683 cm^{-1} that lack sensitivity to NO-isotope labeling must correspond to rearrangement of endogenous ligands to the metal iron center(s) and porphyrin modes perturbations following the photolysis of the nitrite group. Porphyrin and proteinaceous vibrations also contribute differential signals in the 1200 to 1300 cm^{-1} region that overlap with the NO-isotope sensitive signals from the nitrito group. While specific isotope labeling would be required to

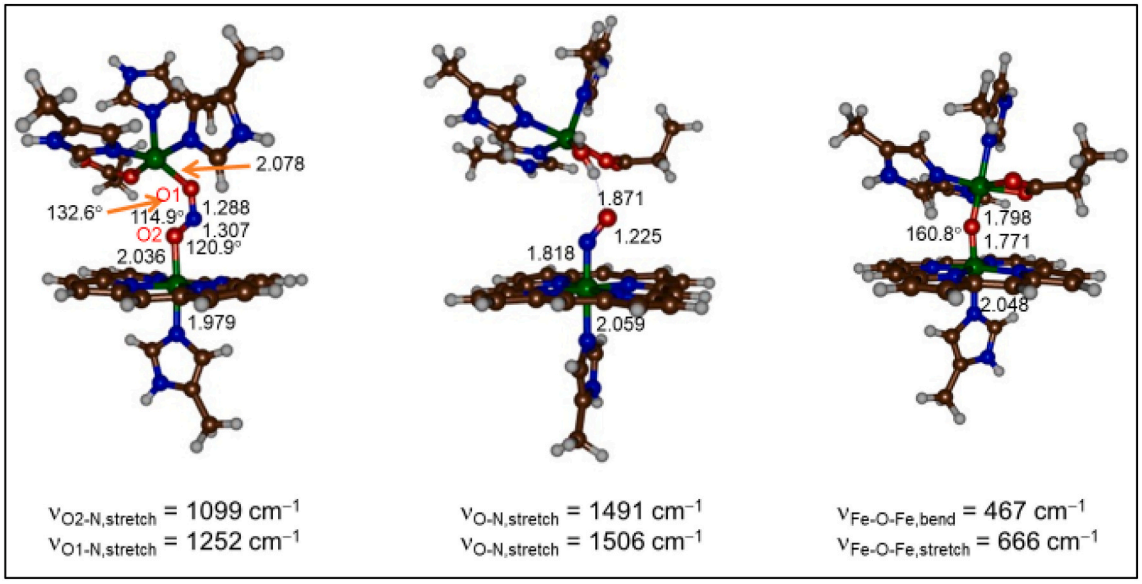

Fig. 6. DFT optimized structures of the nitrite (left), NO (middle), and μ-oxo (right) complexes calculated at the UB3LYP-D level of theory with bond lengths given in angstroms.

provide solid assignment for these modes, the sharpness and intensity of these differential signals further support the notion that the photolysis process observed here is of prominence and mostly homogenous.

FTIR photolysis measurements were also carried out with samples prepared at pH 6 and pH 9, but they produced equivalent difference spectra to those observed at pH 7 (see Supplementary Information).

In an effort to produce additional evidence for the formation of the nitrite adduct, we also performed an experiment with cNOR samples exposed to $^{18}OH_2$ to exchange the μ-oxo bridge prior to reacting with NO. To our surprise, the $^{16/18}$O-exchange of the μ-oxo group has no significant impact on the 1261 cm^{-1} FTIR signal, but thankfully, this lack of sensitivity to the isotope labeling of the μ-oxo group is reproduced for the frequency calculations of our DFT-based bridging nitrito group described below.

Low-temperature FTIR photolysis experiments carried out with oxidized *P.a.* cNOR exposed to NO generated equivalent differential spectra to those obtained with *P.d.* cNOR (Fig. 5).

Because the nitrato complex is expected to be a mixed valence Fe(III)-Fe(II) species, attempts were made to detect EPR signals attributable to this species, but only substochiometric signals could be observed, presumably because of excessive signal broadening (data not shown).

3.4. Density Functional Theory analysis of the binuclear nitrite adduct

Calculations of nitrite, NO and oxo-bridged diiron complexes were performed using the initial coordinates of the diferric μ-oxo cluster used by Blomberg and Siegbahn [14]. The optimized geometry of our model with nitrite bridging the two iron centers in a μ-1,3 fashion (Fig. 6) produced N—O vibrational frequencies that match the experimental FTIR results perfectly. Specifically, the 1261 cm^{-1} FTIR band dependence on NO isotopes and lack of response to ^{18}O-labeling of the μ-oxo bridge is reproduced by a calculated vibration mode at 1252 cm^{-1} that downshifts 22.5 cm^{-1} with ^{15}NO (experimental shift = −25 cm^{-1}), 49 cm^{-1} with $^{15}N^{18}O$ (experimental shift = −55 cm^{-1}), and 3 cm^{-1} with μ-^{18}O (no significant experimental shift). Eigenvectors of this mode are dominated by displacements of the N-atom and O-atom bound to Fe_B. A second calculated mode at 1099 cm^{-1}, below the spectral window of our IR experiment, corresponds to the other N—O stretch of the nitrito group, with calculated shifts for ^{15}NO, $^{15}N^{18}O$, and μ-^{18}O of −20.5, −21.5, and − 24 cm^{-1} respectively. The optimized geometry has a relatively long Fe—O distance of 2.036 Å between heme and NO_2 group while the Fe_B-O1 interaction is 2.078 Å. These are typical metal-ligand interactions and were seen for analogous heme and nonheme iron complexes [50]. By contrast, the μ-oxo-bridged diiron(III) complex and end-on NO-bound heme structure show vibrational frequencies far off from the experimental FTIR frequencies observed here (Fig. 6).

4. Conclusions

On the basis of theoretical calculations, Blomberg and Siegbahn

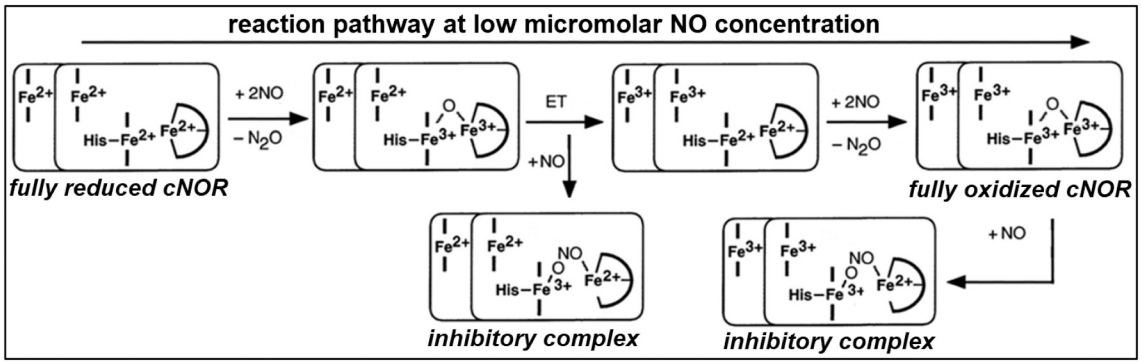

Scheme 2. Mechanism of inhibition in cNORs.

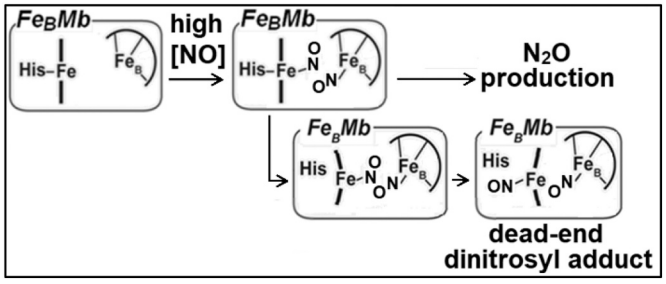

Scheme 3. Production of N_2O in Fe_BMbs and side-reaction leading to a dead-end dinitrosyl complex (adapted from [48,53]).

proposed a substrate-inhibition mechanism initiated by a radical attack of NO on the μ-oxo group bridging the two iron center [14]. Our FTIR photolysis data provide direct support for the formation of a nitrite adduct at the heme-nonheme diiron site upon exposure of oxidized cNOR to NO.

FTIR photolysis measurements performed with ^{18}O-labeled μ-oxo groups indicate that this O-atom remains attached to the heme b_3(III) and that the nitrite group formed upon reaction with NO does not easily isomerize while bound at the diiron center. The lack of negative signal for the nitrite group suggests that after illumination the nitrite group does not remain coordinated to either iron, otherwise it would show distinctive $\nu(NO_2)$, but yet remains unable to rotate within the active site since ^{18}O-shift of the 1261 cm^{-1} band is not observed even after consecutive dissociation/annealing cycles.

Nitrite is not an inhibitor of denitrifying cNORs because these enzymes lack hydrophilic channels to provide anions access to the diiron site, but large hydrophobic channels required for the egress of the N_2O product allow ample access for reversible inhibition by NO. Stopped-flow experiments performed at 80 μM NO show clear evidence of substrate inhibition, with NO reactions at the diiron site preventing electron transfer between the heme b_3:Fe_B diiron site and the low-spin ferrous heme *b* and *c* centers. In view of the reactivity of the diferric μ-oxo bridge cluster toward NO, it is reasonable to assume that substrate inhibition occur after a first half-reaction cycle, validating the Fe(III)-O-Fe(III) active site cluster as the direct product of the NO reduction reaction and supporting the notion that the NO reductive steps of the mechanism do not require protonation of activated Fe-NO species such as iron-nitroxyl or iron-hyponitrite complexes (Scheme 2).

Prior work on engineered myoglobins from the Lu group (formerly at the University of Illinois, now at the University of Texas at Austin) offers an alternative mechanism of substrate inhibition at the heme-nonheme diiron site. These constructs called Fe_BMbs use the scaffold of sperm whale myoglobin and mimic the heme-nonheme diiron site of cNORs by including an Fe_B site in the distal pocket with three histidine and one glutamate residue [51,52]. Stopped-flow UV–vis and rapid-freeze-quenched RR spectroscopic studies by Matsumura et al. [48,53] have shown that diferrous Fe_BMbs can reduce NO to N_2O but that binding of NO at the heme iron(II) can also facilitate dissociation of its proximal histidine to allow formation of a proximally bound five-coordinate heme low-spin nitrosyl complex (Scheme 3).

Because the UV–vis spectra of cNORs are dominated by contributions of its two low-spin hemes, our stopped-flow traces provide limited information on the status of the diiron cluster and whether substrate inhibition is caused by the formation of a heme b_3 Fe(III)-ONO-Fe_B(II) complex or a diiron-dinitrosyl inhibitory complex. Nevertheless, because the rate of inhibition in cNOR exceed the millisecond time resolution of our stopped-flow and sharply contrast with the slow build-up of the dinitrosyl adduct in Fe_BMbs [48,53], our study strongly favors the inhibition mechanism shown in Scheme 2.

Declaration of Competing Interest

The authors declare that they have no known competing financial interests or personal relationships that could have appeared to influence the work reported in this paper.

Acknowledgements

This work was supported by National Institutes of Health Grant R01 GM074785 to P.M.L. and grant NWO–CW 711.014.006 from the Council for Chemical Sciences of The Netherlands Organization for Scientific Research to P.L.H.

Appendix A. Supplementary data

Supplementary data to this article can be found online at https://doi.org/10.1016/j.jinorgbio.2022.111781.

References

[1] C. Schoen, L. Kischkies, J. Elias, B.J. Ampattu, Metabolism and virulence in *Neisseria meningitidis*, Front. Cell. Infect. Microbiol. 4 (2014) 114.
[2] L.Y. Stein, Surveying N_2O-producing pathways in bacteria, in: G.K. Martin (Ed.), Methods Enzym, Academic Press, 2011, pp. 131–152.
[3] K.R. Barth, V.M. Isabella, L.F. Wright, V.L. Clark, Resistance to peroxynitrite in *Neisseria gonorrhoeae*, Microbiology 155 (2009) 2532–2545.
[4] K.R. Barth, V.M. Isabella, V.L. Clark, Biochemical and genomic analysis of the denitrification pathway within the genus *Neisseria*, Microbiology 155 (2009) 4093–4103.
[5] T. Hino, Y. Matsumoto, S. Nagano, H. Sugimoto, Y. Fukumori, T. Murata, S. Iwata, Y. Shiro, Structural basis of biological N_2O generation by bacterial nitric oxide reductase, Science 330 (2010) 1666–1670.
[6] P. Moënne-Loccoz, O.-M.H. Richter, H.W. Huang, I.M. Wasser, R.A. Ghiladi, K. D. Karlin, S. de Vries, Nitric oxide reductase from *Paracoccus denitrificans* contains an oxo-bridged heme/non-heme diiron center, J. Am. Chem. Soc. 122 (2000) 9344–9345.
[7] C.F. Martens, N.N. Murthy, H.V. Obias, K.D. Karlin, Oxo-bridged haem/non-haem iron complexes, J. Chem. Soc. Chem. Commun. (1996) 629–630.
[8] P. Moënne-Loccoz, S. de Vries, Structural characterization of the catalytic high-spin heme *b* of nitric oxide reductase: a resonance Raman study, J. Am. Chem. Soc. 120 (1998) 5147–5152.
[9] P. Girsch, S. de Vries, Purification and initial kinetic and spectroscopic characterization of NO reductase from *Paracoccus denitrificans*, Biochim. Biophys. Acta 1318 (1997) 202–216.
[10] N. Sato, S. Ishii, H. Sugimoto, T. Hino, Y. Fukumori, Y. Sako, Y. Shiro, T. Tosha, Structures of reduced and ligand-bound nitric oxide reductase provide insights into functional differences in respiratory enzymes, Proteins 82 (2014) 1258–1271.
[11] W.R. Hagen, Hypothesis: entatic versus ecstatic states in metalloproteins, Metallomics 11 (2019) 1768–1778.
[12] P. Moënne-Loccoz, Spectroscopic characterization of heme iron-nitrosyl species and their role in NO reductase mechanisms in diiron proteins, Natl. Prod. Rep. 24 (2007) 610–620.
[13] L.M. Blomberg, M.R. Blomberg, P.E.M. Siegbahn, Reduction of nitric oxide in bacterial nitric oxide reductase-a theoretical model study, Biochim. Biophys. Acta 1757 (2006) 240–252.
[14] M.R. Blomberg, P.E.M. Siegbahn, Mechanism for N_2O generation in bacterial nitric oxide reductase: a quantum chemical study, Biochemistry 51 (2012) 5173–5186.
[15] M.R. Blomberg, Can reduction of NO to N_2O in cytochrome c dependent nitric oxide reductase proceed through a trans-mechanism? Biochemistry 56 (2017) 120–131.
[16] E. Terasaka, N. Okada, N. Sato, Y. Sako, Y. Shiro, T. Tosha, Characterization of quinol-dependent nitric oxide reductase from *Geobacillus stearothermophilus*: enzymatic activity and active site structure, Biochim. Biophys. Acta 7 (2014) 22.
[17] H. Takeda, T. Kimura, T. Nomura, M. Horitani, A. Yokota, A. Matsubayashi, S. Ishii, Y. Shiro, M. Kubo, T. Tosha, Timing of NO binding and protonation in the catalytic reaction of bacterial nitric oxide reductase as established by time-resolved spectroscopy, Bull. Chem. Soc. Jpn. 93 (2020) 825–833.
[18] H. Kumita, K. Matsuura, T. Hino, S. Takahashi, H. Hori, Y. Fukumori, I. Morishima, Y. Shiro, NO reduction by nitric oxide reductase from denitrifying bacterium *Pseudomonas aeruginosa*: characterization of reaction intermediates that appear in the single turnover cycle, J. Biol. Chem. 279 (2004) 55247–55254.
[19] M. Koutny, I. Kucera, Kinetic analysis of substrate inhibition in nitric oxide reductase of *Paracoccus denitrificans*, Biochem. Biophys. Res. Commun. 262 (1999) 562–564.
[20] E. Pinakoulaki, S. Gemeinhardt, M. Saraste, C. Varotsis, Nitric-oxide reductase. Structure and properties of the catalytic site from resonance Raman scattering, J. Biol. Chem. 277 (2002) 23407–23413.
[21] T. Hino, S. Nagano, H. Sugimoto, T. Tosha, Y. Shiro, Molecular structure and function of bacterial nitric oxide reductase, Biochim. Biophys. Acta 1817 (2012) 680–687.

[22] S. Lu, S. de Vries, P. Moënne-Loccoz, Two CO molecules can bind concomitantly at the diiron site of NO reductase from *Bacillus azotoformans*, J. Am. Chem. Soc. 126 (2004) 15332–15333.

[23] S. Lu, M.H. Sazinsky, J.W. Whittaker, S.J. Lippard, P. Moënne-Loccoz, Fourier transform infrared characterization of the azido complex of methane monooxygenase hydroxylase from *Methylococcus capsulatus* (Bath), J. Am. Chem. Soc. 127 (2005) 4148–4149.

[24] T. Hayashi, I.J. Lin, Y. Chen, J.A. Fee, P. Moënne-Loccoz, Fourier transform infrared characterization of a Cu_B-nitrosyl complex in cytochrome ba_3 from *Thermus thermophilus*: relevance to NO reductase activity in heme-copper terminal oxidases, J. Am. Chem. Soc. 129 (2007) 14952–14958.

[25] T. Hayashi, M.T. Lin, K. Ganesan, Y. Chen, J.A. Fee, R.B. Gennis, P. Moënne-Loccoz, Accommodation of two diatomic molecules in cytochrome *bo*: insights into NO reductase activity in terminal oxidases, Biochemistry 48 (2009) 883–890.

[26] T. Hayashi, J.D. Caranto, H. Matsumura, D.M. Kurtz Jr., P. Moënne-Loccoz, Vibrational analysis of mononitrosyl complexes in hemerythrin and flavodiiron proteins: relevance to detoxifying NO reductase, J. Am. Chem. Soc. 134 (2012) 6878–6884.

[27] (a)Jaguar, V., Schrodinger, LLC: New York, NY, 2011. (b) M.J. Frisch, et al., Gaussian 09, Revision D.01, Gaussian Inc., Wallingford, CT, 2010.

[28] S. Louka, S.M. Barry, D.J. Heyes, M.Q.E. Mubarak, H.S. Ali, L.M. Alkhalaf, A. W. Munro, N.S. Scrutton, G.L. Challis, S.P. de Visser, Catalytic mechanism of aromatic nitration by cytochrome P450 TxtE: involvement of a ferric-peroxynitrite intermediate, J. Am. Chem. Soc. 142 (2020) 15764–15779.

[29] H.S. Ali, R.H. Henchman, J. Warwicker, S.P. de Visser, How do electrostatic perturbations of the protein affect the bifurcation pathways of substrate hydroxylation versus desaturation in the nonheme iron-dependent viomycin biosynthesis enzyme? J. Phys. Chem. A 125 (2021) 1720–1737.

[30] A.D. Becke, Density-functional thermochemistry. III. The role of exact exchange, J. Chem. Phys. 98 (1993) 5648–5652.

[31] P.J. Hay, W.R. Wadt, Ab initio effective core potentials for molecular calculations. Potentials for the transition metal atoms scandium to mercury, J. Chem. Phys. 82 (1985) 270–283.

[32] T. Sakurai, N. Sakurai, H. Matsumoto, S. Hirota, O. Yamauchi, Roles of four iron centers in *Paracoccus halodenitrificans* nitric oxide reductase, Biochem. Biophys. Res. Commun. 251 (1998) 248–251.

[33] M.R. Cheesman, W.G. Zumft, A.J. Thomson, The MCD and EPR of the heme centers of nitric oxide reductase from *Pseudomonas stutzeri*: evidence that the enzyme is structurally related to the heme-copper oxidases, Biochemistry 37 (1998) 3994–4000.

[34] C.G. Timoteo, A.S. Pereira, C.E. Martins, S.G. Naik, A.G. Duarte, J.J. Moura, P. Tavares, B.H. Huynh, I. Moura, Low-spin heme b_3 in the catalytic center of nitric oxide reductase from *Pseudomonas nautica*, Biochemistry 50 (2011) 4251–4262.

[35] A.G. Duarte, C.M. Cordas, J.J. Moura, I. Moura, C.M. Cordas, A.G. Duarte, J. J. Moura, I. Moura, C.G. Timoteo, A.S. Pereira, C.E. Martins, S.G. Naik, A. G. Duarte, J.J. Moura, P. Tavares, B.H. Huynh, I. Moura, Steady-state kinetics with nitric oxide reductase (NOR): new considerations on substrate inhibition profile and catalytic mechanism, Biochim. Biophys. Acta 1837 (2014) 375–384.

[36] J.O. Alben, P.P. Moh, F.G. Fiamingo, R.A. Altschuld, Cytochrome oxidase a_3 heme and copper observed by low-temperature Fourier transform infrared spectroscopy of the CO complex, Proc. Natl. Acad. Sci. U. S. A. 78 (1981) 234–237.

[37] J.O. Alben, D. Beece, S.F. Bowne, W. Doster, L. Eisenstein, H. Frauenfelder, D. Good, J.D. McDonald, M.C. Marden, P.P. Moh, L. Reinisch, A.H. Reynolds, E. Shyamsunder, K.T. Yue, Infrared spectroscopy of photodissociated carboxymyoglobin at low temperatures, Proc. Natl. Acad. Sci. U. S. A. 79 (1982) 3744–3748.

[38] F.G. Fiamingo, J.O. Alben, Structures of photolyzed carboxymyoglobin, Biochemistry 24 (1985) 7964–7970.

[39] A. Ansari, J. Berendzen, D. Braunstein, B.R. Cowen, H. Frauenfelder, M.K. Hong, I. E.T. Iben, J.B. Johnson, P. Ormos, T.B. Sauke, R. Scholl, A. Schulte, P.J. Steinbach, J. Vittitow, R.D. Young, Rebinding and relaxation in the myoglobin pocket, Biophys. Chem. 26 (1987) 337–355.

[40] H. Hori, M. Ikeda-Saito, G. Lang, T. Yonetani, Electronic and stereochemical characterizations of the photoinduced intermediates of nitrosyl complexes of metal ($S = 5/2$)-substituted hemoproteins trapped at low temperature, J. Biol. Chem. 265 (1990) 15028–15033.

[41] L.M. Miller, A.J. Pedraza, M.R. Chance, Identification of conformational substates involved in nitric oxide binding to ferric and ferrous myoglobin through difference Fourier transform infrared spectroscopy (FTIR), Biochemistry 36 (1997) 12199–12207.

[42] H. Hori, F. Masuya, Y. Dou, M. Ikeda-Saito, EPR studies on the photoinduced intermediates of NO complexes in recombinant ferric-Mb trapped at low temperatures, J. Inorg. Biochem. 82 (2000) 181–187.

[43] S. Lu, E. Libby, L. Saleh, G. Xing, J.M. Bollinger Jr., P. Moënne-Loccoz, Characterization of NO adducts of the diiron center in protein R2 of *Escherichia coli* ribonucleotide reductase and site-directed variants. Implications for the O_2-activation mechanism, J. Biol. Inorg. Chem. 9 (2004) 818–827.

[44] T. Hayashi, K.D. Miner, N. Yeung, Y.W. Lin, Y. Lu, P. Moënne-Loccoz, Spectroscopic characterization of mononitrosyl complexes in heme–nonheme diiron centers within the myoglobin scaffold (Fe_BMbs): relevance to denitrifying NO reductase, Biochemistry 50 (2011) 5939–5947.

[45] Z.N. Nilsson, B.L. Mandella, K. Sen, D. Kekilli, M.A. Hough, P. Moënne-Loccoz, R. W. Strange, C.R. Andrew, Distinguishing nitro vs nitrito coordination in cytochrome c' using vibrational spectroscopy and density functional theory, Inorg. Chem. 56 (2017) 13205–13213.

[46] T.S. Kurtikyan, A.A. Hovhannisyan, G.M. Gulyan, P.C. Ford, Interaction of nitrogen bases with iron-porphyrin nitrito complexes Fe(Por)(ONO) in sublimed solids, Inorg. Chem. 46 (2007) 7024–7031.

[47] G.M. Gulyan, T.S. Kurtikyan, P.C. Ford, Six-coordinate nitrato complexes of iron (III) porphyrins, Inorg. Chem. 47 (2008) 787–789.

[48] H. Matsumura, T. Hayashi, S. Chakraborty, Y. Lu, P. Moënne-Loccoz, The production of nitrous oxide by the heme/nonheme diiron center of engineered myoglobins (Fe_BMbs) proceeds through a trans-iron-nitrosyl dimer, J. Am. Chem. Soc. 136 (2014) 2420–2431.

[49] A. Bhagi-Damodaran, J.H. Reed, Q. Zhu, Y. Shi, P. Hosseinzadeh, B.A. Sandoval, K. A. Harnden, S. Wang, M.R. Sponholtz, E.N. Mirts, S. Dwaraknath, Y. Zhang, P. Moënne-Loccoz, Y. Lu, Heme redox potentials hold the key to reactivity differences between nitric oxide reductase and heme-copper oxidase, Proc. Natl. Acad. Sci. U. S. A. 115 (2018) 6195–6200.

[50] G. Mukherjee, J.K. Satpathy, U.K. Bagha, M. Qadri, E. Mubarak, C.V. Sastri, S.P. de Visser, Inspiration from nature: influence of engineered ligand scaffolds and auxiliary factors on the reactivity of biomimetic oxidants, ACS Catal. 11 (2021) 9761–9797.

[51] Y.W. Lin, N. Yeung, Y.G. Gao, K.D. Miner, S. Tian, H. Robinson, Y. Lu, Roles of glutamates and metal ions in a rationally designed nitric oxide reductase based on myoglobin, Proc. Natl. Acad. Sci. U. S. A. 107 (2010) 8581–85816.

[52] N. Yeung, Y.W. Lin, Y.G. Gao, X. Zhao, B.S. Russell, L. Lei, K.D. Miner, H. Robinson, Y. Lu, Rational design of a structural and functional nitric oxide reductase, Nature 462 (2009) 1079–1082.

[53] H. Matsumura, S. Chakraborty, J. Reed, Y. Lu, P. Moënne-Loccoz, Effect of outer-sphere side chain substitutions on the fate of the *trans* iron-nitrosyl dimer in heme/nonheme engineered myoglobins (Fe_BMbs): insights into the mechanism of denitrifying NO reductases, Biochemistry 55 (2016) 2091–2099.